Research paper   **Open Access**

Effect of Synthetic Route on the Structure and Morphology of ZnM$_2$O$_4$, M= (Fe, Cr, Mn, Al) Nano-oxides

M. Khairy[1, 2], M. Sameeh[1,*], T. Esawy[1], W. A. Bayoumy[1]

[1]Chemistry Department, Faculty of Science, Benha University, Benha, Egypt.
[2]Chemistry Department, College of Science, Al-Imam Mohammad Ibn Saud lslamic University, Riyadh, KSA
*Corresponding author: E-mail: Marwa_sameeh@yahoo.com, Tel: 01285777206

Abstract

Nano-crystalline ZnM$_2$O$_4$, M= (Al, Fe, Cr, Mn) particles have been prepared by different methods such as combustion, hydrothermal and sol-gel methods. The samples were characterized by X-ray diffraction (XRD) analysis, Fourier transform infrared spectroscopy (FTIR) and Transmission Electron Microscope (TEM). The XRD analysis showed that the samples exhibit different crystal phases depending on the preparation route. It showed that pure spinel phases formed only by combustion method with crystallite sizes lie in the range of 6 – 37 nm. The particulate and morphological properties have been investigated using TEM techniques.

1. Introduction

Oxide spinels having the general formula AB$_2$O$_4$ [1-3] represent a large class of inorganic materials which exhibit various technological applications including ferrofluids [4], high-density magnetic recording media [5], biomedicine [6] and radar-absorbent materials [7], pigments, refractory, catalysts and electronic ceramics [8]. The fabrication of spinel-structured ferrite at the nano-scale has been intensively investigated in recent years due to their unique physical and chemical properties not found in the more limited binary oxides. They exhibit interesting structural, electrical, magnetic and catalytic properties. Zinc aluminate spinel ZnAl$_2$O$_4$ may be used as a catalytic as well as a ceramic material. So far, it has been used as a catalyst for several organic reactions [9-12]. Zinc aluminate is commonly synthesized by high temperature calcination of mixed aluminium and zinc oxides [13], co-precipitated products [14]. A disadvantage of such materials for catalytic applications is the low surface area [15]. Good results may be obtained by sol-gel methods [16]. As one of the important mixed transition-metal oxides with spinel structure, ZnMn$_2$O$_4$ is a promising functional material and has become the focus of various researches owing to its interesting applications. ZnMn$_2$O$_4$ could be used for the negative temperature coefficient thermistors on account of their unique electrical properties [17]. Ferrari and the coworkers studied the catalytic activity of zinc manganite for the reduction of NO by several types of hydrocarbons [18,19].

Zinc chromium oxide ZnCr$_2$O$_4$ spinel structure, with tetrahedral sites occupied by Zn atoms and octahedral sites occupied by Cr atoms. It can be used in several applications such as gas sensing [20], humidity sensing [21-23], and magnetic properties [24] of the products prepared by these methods were also reported.

There are different methods for synthesize ZnM$_2$O$_4$, M= (Al, Fe, Cr, Mn) such as combustion method which is useful to achieve the fabrication of magnetic nano-ferrites at low annealing temperature. The size and morphology of nano particles and their properties can be controlled by modifying the composition of the nano-composites. Synthesis of nano-crytalline materials by hydrothermal technique is most useful due to its simplicity, low cost and nontoxic route. Furthermore, it offers the possibility to deal with a great number of experimental strategies by modification of parameters such as solvent, precipitant agent concentration or temperature. The main advantages of sol gel method, as compared to traditional methods, are lower processing temperatures, control over purity, composition and easy introduction of doping elements [25-27].

In the present paper we study the effect of different synthetic methods with different thermal treatments on the structure, particle size and the morphological structure of ZnM$_2$O$_4$, M= (Al, Fe, Cr, Mn) nanoparticles.

2. Experimental

2.1. Materials

All chemical used were good reagent and used without moreover purification. Aluminum nitrate [Al(NO$_3$)$_3$.9H$_2$O, 99.9%], Zinc nitrate (Hexahydrat) [Zn (NO$_3$)$_2$.6H$_2$O], and Manganese acetate [Mn(CH$_3$COO)$_2$.4H$_2$O, 98.5%] were

purchased from LOBA CHEMIE PVT.LTD, Mumbai-400005.INDIA. Ferric nitrate [$Fe(NO_3)_3.9H_2O$, 99.95%] was gotten from Oxford Laboratory, Mumbai 400005. Chromium nitrate [$Cr(NO_3)_3.9H_2O$, 99%] was acquired from Qualikems Fine Chemicals PVT.LTD. Manganese nitrate [$Mn(NO_3)_2.4H_2O$, 98%] was obtained from Chem-Lab NV. Zinc acetate [$(CH_3COO)_2Zn.2H_2O$, 98%], potassium hydroxide (KOH) and glycine ($NH_2.CH_2.COOH$) were purchased from A Dwic, EL Nasr pharmaceutical chemicals-CO, Egypt. Citric acid ($C_6H_8O_7.H_2O$) was obtained from VEB Berlin. Chemie. Distilled water was used throughout the whole experiments.

2.2. Synthesis of materials

Samples with the composition ZnM_2O_4, M= (Al, Fe, Cr, Mn) were synthesized by various methods such as combustion, hydrothermal and sol-gel methods.

2.2.1. Combustion Method

In a typical experiment, $ZnAl_2O_4$, $ZnFe_2O_4$, $ZnCr_2O_4$ and $ZnMn_2O_4$ powders were synthesized by solution combustion route using the appropriate starting regents of metal nitrates and glycine as a fuel. Glycine possesses a high heat of combustion. It is an organic fuel providing a platform for redox reactions during the course of combustion. For all materials, metal nitrates and glycine are taken in the 1:2:4.44 stoichiometric amounts and then dissolved in minimum quantity of distilled water. The mixed solution was evaporated on hot plate at about 100 °C for auto-combustion. Initially the solution foils boil and undergoes dehydration followed by decomposition with evolution of gases (N_2 and CO_2). Then, it burns to yield voluminous and foamy homogeneous residue. During the burning reaction, the flame temperature is reported to be above 1000°C. The resulting materials are pulverized and calcined at 400°C for 2 h.

2.2.2. Hydrothermal Method

In the hydrothermal method, stoichiometric amounts of ($Zn(CH_3COO)_2.2H_2O$ and $Al(NO_3)_3.9H_2O$); ($Zn(NO_3)_2.6H_2O$ and $Fe(NO_3)_3.9H_2O$); ($Zn(NO_3)_2.6H_2O$ and $Cr(NO_3)_3.9H_2O$); ($Zn(CH_3COO)_2.2H_2O$ and $Mn(CH_3COO)_2.4H_2O$) were used to prepare 0.02 mole of $ZnAl_2O_4$, $ZnFe_2O_4$, $ZnCr_2O_4$ and $ZnMn_2O_4$, respectively. The appropriate amounts of mixed materials were dissolved in 50 ml distilled water, then 25 ml of SDS as surfactant ($5×10^{-3}$ M) was added. The mixed solution was stirred well using a magnetic stirrer at room temperature until the solution became transparent. By adding a NaOH (2M) slowly drop by drop with continuous stirring until pH = 11, the corresponding metal hydroxides were precipitated. This precipitate was transferred into a Teflon stainless-steal autoclave and heated at: 170°C for 8 h [for $ZnAl_2O_4$]; 160°C for 15 h [for $ZnFe_2O_4$]; 220°C for 48 h [for $ZnCr_2O_4$] and 170°C for 8 h [for $ZnMnO_4$]. After the autoclave was cooled down to room temperature naturally, the precipitated was collected by centrifugation and washed with distilled water and anhydrous ethanol several times to remove possible impurities or excess ions. The powder was then dried at 80°C, finally the resulting powder is calcined at 400°C for 2 h.

2.2.3. Sol-gel Method

For preparing 0.1 mol of $ZnAl_2O_4$, $ZnFe_2O_4$, $ZnCr_2O_4$ and $ZnMn_2O_4$, the corresponding metal nitrate mentioned above were mixed with citric acid in the molar ratio 1:2:2.22 and then 25 ml of SDS as surfactant ($5×10^{-3}$ M) was added. The mixed solution was heated at 80°C under continuously stirring to remove the excess of the solvent. The obtained gel was sintered in air at 200°C for 1 h until a viscous wet gel was obtained. The resultant powder was calcined in a furnace at 400°C for 2 h.

2.3. Characterization

2.3.1. X-ray diffraction (XRD)

X-ray diffraction (XRD) was measured at room temperature by using a Philips diffract meter 321/00 instrument. The patterns were progressed with Ni-filtered copper radiation (λ= 1.541 Å) at 36 kV and 10 mA with a scanning speed of 2θ= 5°/min.

2.3.2. Fourier transform infrared spectroscopy (FTIR)

The Fourier transform infrared (FTIR) spectra were monitored via a double beam Perkin Elmer Spectrometer (Thermo scientific Nicolet iS10), with a resolution of 2 cm^{-1}, using KBr method. The samples were grounded with KBr (1:100) to form tablets and thus confined into the sample holder in the spectrometer cavity to record the measurements in the 4000–400 cm^{-1} region.

2.3.3. Scanning electron microscope (SEM)

The surface morphologies of the prepared samples were analyzed by a scanning electron microscope (SEM, JEOL-JSM 6360 unit).

2.3.4. Transmission Electron Microscope (TEM)

TEM is a good tool to study the particle size and morphology. TEM gives a good resolution down to a nanometer scale. Photographs were taken using transmission electron microscope TEM (Philips CM-12 unit).

3. Results and Discussion

3.1. X-ray diffraction (XRD)

The XRD of $ZnAl_2O_4$, $ZnFe_2O_4$, $ZnCr_2O_4$, and $ZnMn_2O_4$ synthesized by combustion method are shown in Figs. 1, 2. Before annealing, the XRD of $ZnAl_2O_4$, $ZnFe_2O_4$ and $ZnCr_2O_4$ samples showed reflection planes of (220), (311), (400), (422), (511) and (440) indicating to spinel structure of $ZnAl_2O_4$, $ZnFe_2O_4$ and $ZnCr_2O_4$ according to the standard JCPDS cards no. (05-0669), (22-1012), (22-1107), respectively with some traces of AlO(OH) with $ZnAl_2O_4$ phase and ZnO_2 with $ZnFe_2O_4$ according to the standard JCPDS cards no. (76-1871) and (13-311), While the XRD pattern for $ZnMn_2O_4$ sample showed reflection planes of (101), (112), (103), (211), (224) and (400) indicating to pure spinel structure of $ZnMn_2O_4$ according to the standard JCPDS cards no. (24-1133) with some oxides of Mn_3O_4 and Mn_2O_3 according to the standard JCPDS cards no. (24-0734) and (41-1442). After annealing at 400°C, all compounds show pure spinel crystal structure. No other different peaks are observed for all specimens showing the purity of the spinels prepared by the combustion method.
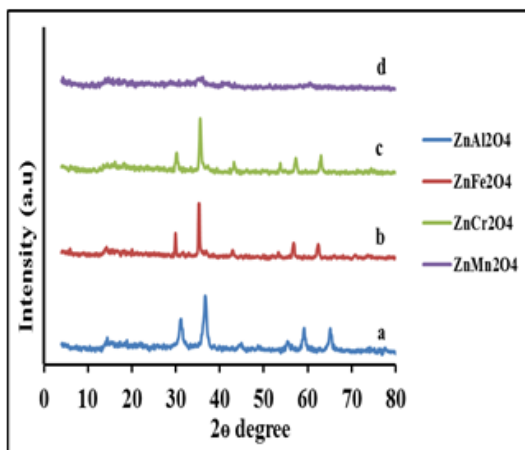
Fig.1: X-ray diffraction patterns for ZnM_2O_4, where M=Al, Fe, Cr and Mn have been prepared by the combustion method at room temperature.

Fig.2: X-ray diffraction patterns for ZnM_2O_4, where M=Al, Fe, Cr and Mn have been prepared by the combustion method calcined at 400°C.

The XRD of the samples prepared by hydrothermal method are shown in Figs. 3, 4. The XRD of $ZnAl_2O_4$ sample showed mixed phases of $Zn(OH)_2$, $Zn(C_2H_3O_2)_2.2H_2O$, $Zn.(H_2O)_6(NO_3)_2$ and $Al(NO_3)_3.9H_2O$ according to the standard JCPDS cards no. (38-0385), (01-0215), (72-0058) and (24-0004), respectively. The XRD of synthesized $ZnCr_2O_4$ and $ZnFe_2O_4$ samples showed pure spinel structure. Whereas, XRD of $ZnMn_2O_4$ sample showed mixed phases of ZnO, $(H_5O_2)(Mn(H_2O)_2(SO_4)_2)$, MnO_2 and $Mn_2(CO)_{10}$

according to the standard JCPDS cards no. (36-1451), (76-1451), (18-0802) and (74-0853), respectively. XRD of all calcined samples, at 400°C for 2 h, showed the formation of pure spinel structure. But the $ZnMn_2O_4$ sample demonstrated, in addition to the main spinel peaks, some small peaks attributed to the presence of ZnO with the hexagonal wurtzite-structured (P63mc) as indexed in the standard data (JCPDS card No. 36-1451, a = 3.249 A˚and c = 5.206 A˚) [28].
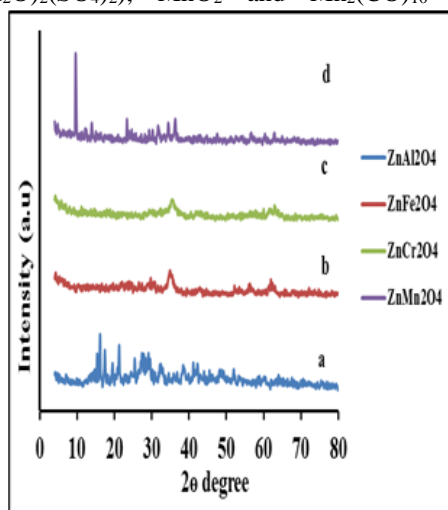

Fig.3: X-ray diffraction patterns for ZnM_2O_4, where M=Al, Fe, Cr and Mn have been prepared by the hydrothermal method at room temperature.

Fig.4: X-ray diffraction patterns for ZnM_2O_4, where M=Al, Fe, Cr and Mn have been prepared by the hydrothermal method at 400°C.

The XRD of the samples prepared by sol-gel method are given in Figs. 5, 6. The XRD of as prepared $ZnAl_2O_4$, $ZnCr_2O_4$ and $ZnFe_2O_4$ samples showed amorphous structure. While XRD of $ZnMn_2O_4$ sample showed mixed oxides phases of MnO, Mn_3O_4 and ZnO according to the standard JCPDS cards no. (75-0626), (24-0734) and (36-1451). After calcination at 400°C, the XRD of $ZnAl_2O_4$ sample
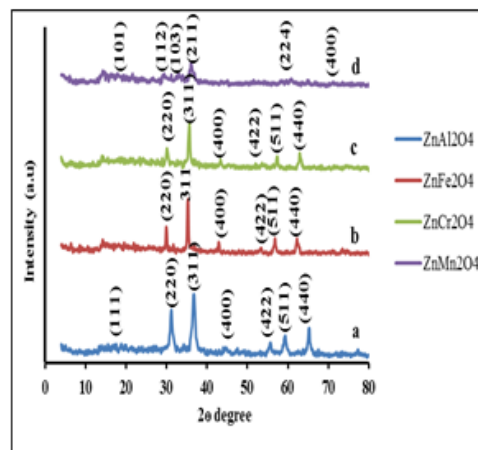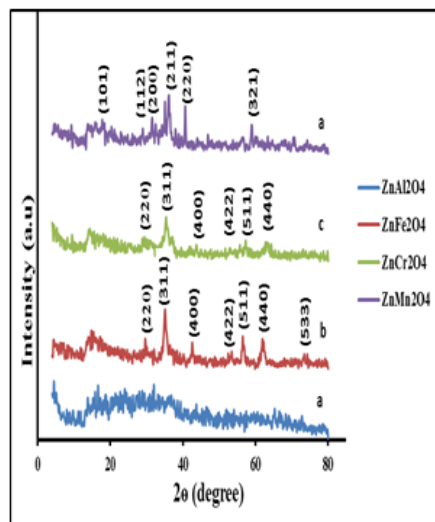
demonstrates an amorphous structure and pure spinel structure for $ZnFe_2O_4$. While XRD of $ZnCr_2O_4$ sample showed mixed phases of $ZnCr_2O_4$ spinel and traces of ZnO_2 with cubic structure with space group of Pa3 (JCPDS file 13-311). Whereas, the XRD of $ZnMn_2O_4$ sample showed mixed oxides phases of MnO, Mn_3O_4 and ZnO. All phases produced by the different methods are summarized in Table 1.
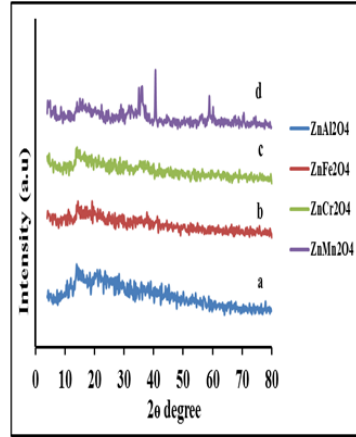
Fig.5: X-ray diffraction patterns for ZnM_2O_4, where M=Al, Fe, Cr and Mn have been prepared by the sol-gel method at room temperature.
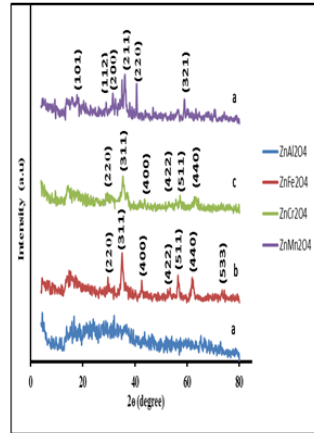

Fig. 6: X-ray diffraction patterns for ZnM_2O_4, where M=Al, Fe, Cr and Mn have been prepared by the sol-gel method calcined at 400°C.

Table (1): The XRD data for all samples synthesized with different preparation methods.

Samples	Hydrothermal Method		Combustion method		Sol gel method	
	Phases	Particle size	phases	Particle size	phases	Particle size
$ZnAl_2O_4$ before annealing	$Zn(OH)_2$ $Zn(C_2H_3O_2)_2.2H_2O$ $Zn. (H_2O)_6 (NO_3)_2$ $Al(NO_3)_3.9 H_2O$	48	$ZnAl_2O_4$ (spinel) $AlO(OH)$	12	Amorphous	-
$ZnAl_2O_4$ 400	$ZnAl_2O_4$ (spinel)	8	$ZnAl_2O_4$(spinel)	15	Amorphous	-
$ZnCr_2O_4$ before annealing	$ZnCr_2O_4$ (spinel)	6	$ZnCr_2O_4$ (spinel)	36	Amorphous	-
$ZnCr_2O_4$ 400	$ZnCr_2O_4$ (spinel)	19	$ZnCr_2O_4$ (spinel)	29	$ZnCr_2O_4$(spinel) ZnO_2(cubic)	27
$ZnFe_2O_4$ before annealing	$ZnFe_2O_4$ (spinel)	23	$ZnFe_2O_4$ (spinel) ZnO_2(cubic)	51	Amorphous	-
$ZnFe_2O_4$ 400	$ZnFe_2O_4$ (spinel)	19	$ZnFe_2O_4$ (spinel)	70	$ZnFe_2O_4$(spinel)	30
$ZnMn_2O_4$ before annealing	ZnO(hexagonal) $(H_5O_2)(Mn(H_2O)_2$ $(SO_4)_2)$ MnO_2 $Mn_2(CO)_{10}$	55	$ZnMn_2O_4$ (spinel) Mn_3O_4 (tetragonal) Mn_2O_3	8	MnO(cubic) Mn_3O_4 (tetragonal) ZnO (hexagonal)	35
$ZnMn_2O_4$ 400	$ZnMn_2O_4$(spinel) ZnO(hexagonal)	34	$ZnMn_2O_4$ (spinel)	5	MnO(cubic) Mn_3O_4 (tetragonal) ZnO (hexagonal)	43

The average crystallite sizes of the samples designed from the most intense diffraction peak in all prepared materials using the Debye–Scherrer equation [29] and also given in Table 1.

According to the variation method, we determined the most intense growth plane formed in the spinel structure by determining the texturing coefficient using the following equation:

$$TC = \frac{I_{(hkl)}/I_{0(hkl)}}{\frac{1}{N}\sum I_{(hkl)}/I_{0(hkl)}}$$

where $I_{(hkl)}$ and $I_{o(hkl)}$ are the measured intensity and standard integrated intensity for *(hkl)* reflection, respectively, and *N* is the number of reflections observed. The results obtained are registered in Table 1. From which it can be obviously that the prefer plane growth depend on the preparation method. For $ZnAl_2O_4$, in case of hydrothermal method the prefer plane growth is (440), but for combustion method is (111).

For $ZnCr_2O_4$, in case of hydrothermal method the prefer plane growth is (400) and for sol-gel is (422), and for combustion method is (111). For $ZnFe_2O_4$, in case of hydrothermal method the prefer plane growth is (400) and for

sol-gel is (422), and for combustion method is (200). For ZnMn$_2$O$_4$, in case of hydrothermal method, sol-gel method and combustion method, we found the prefer plane growth is (101).

Table (2): Texture Coefficients (TC) of ZnAl$_2$O$_4$, ZnCr$_2$O$_4$, ZnFe$_2$O$_4$ and ZnMn$_2$O$_4$ spinel samples.

Samples	Hydrothermal		Sol gel		Combustion	
	hkl	TC	hkl	TC	hkl	TC
	220	0.65	-	-	111	3.42
	311	1.13	-	-	220	0.46
	511	0.83	-	-	311	0.53
	440	1.37	-	-	422	0.48
	-	-	-	-	511	0.44
ZnAl$_2$O$_4$	-	-	-	-	440	0.53
	-	-	-	-	400	1.11
	220	0.83	220	0.83	220	1.04
	311	0.91	311	0.72	311	0.99
	400	1.22	400	1.37	400	1.19
	511	0.84	422	1.59	511	0.81
	440	1.19	511	0.75	440	0.86
	220	0.83	220	0.86	220	1.41
	311	0.79	311	0.65	311	1.06
ZnFe$_2$O$_4$	400	1.16	400	1.25	400	1.19
	511	1.06	422	1.36	422	0.89
	440	1.13	511	1.02	511	0.75
	-	-	440	0.83	440	0.67
	224	0.68	101	2.69	101	3.15
	211	1.07	112	0.44	112	0.66
	103	0.61	103	0.33	103	0.48
ZnMn$_2$O$_4$	112	0.41	211	0.52	211	0.57
	101	2.23	-	-	224	0.43
	-	-	-	-	400	0.68

From the results above, it can be seen that the phases and crystal sizes formed in our samples depend on the preparation method. The samples prepared by combustion method showed the formation of pure spinel structure and crystallite size in the range of nano size. Therefore, we used the samples prepared by combustion method to investigate the FT-IR, SEM and TEM techniques.

Fig.7: FT-IR spectra for (a) ZnAlO$_4$, (b) ZnFe$_2$O$_4$,(C) ZnCr$_2$O$_4$(d) ZnMn$_2$O$_4$ prepared by combustion method.

3.2. FT-IR

The FT-IR spectra of ZnM$_2$O$_4$, M= (Al, Fe, Cr, Mn) in the range of 200 to 4000 cm^{-1} are shown in Fig. 7. The existence of two main absorption peaks ν_1 and ν_2 characteristic of spinel structure is confirmed for all samples. The values of ν_1 and ν_2 lie in the range (544-660) cm^{-1} and (390-514) cm^{-1}, respectively. The FT-IR spectrum displays a shift in position peaks of both ν_1 and ν_2 wavenumbers associated with several factors, for example, the variations in the metal-oxygen spaces, ionic radii, and the force constants at the tetrahedral- and octahedral- sites. These values matched well with those registered for other spinel systems [30- 34]. The absorption broad bands detected at 3422, 3424 and 3426 cm^{-1} represent the stretching mode of H$_2$O molecules adsorbed on the surface of oxides and OH groups. The force constants corresponding to tetrahedral (F_T) and octahedral positions (F_O) were calculated according to equations (1and 2) and listed in Table 3.
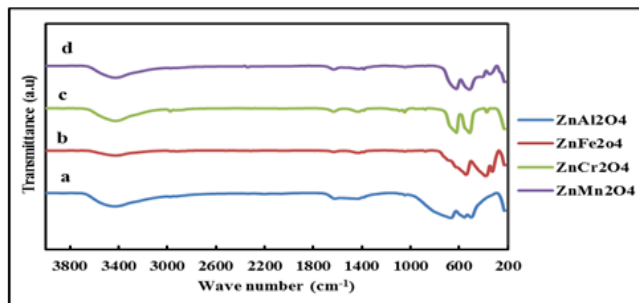
The force constant for the tetrahedral site (k_t) and octahedral site (k_o) was estimated by employing the method suggested by 'Waldron' [35]:

$$K_t = 7.62 \times M_1 \times \nu_1^2 \times 10^{-3} \qquad dyne\ cm^{-1} \qquad (1)$$

$$K_o = 10.62 \times \frac{M_2}{2} \times \nu_2^2 \times 10^{-3} \qquad dyne\ cm^{-1} \qquad (2)$$

Where M_1 and M_2 are the molecular weights of cations on the A- and B-sites, respectively. The results obtained are listed in Table 3, which shows that the force constants in both sites increases in the following order ZnFe$_2$O$_4$ < ZnCr$_2$O$_4$ < ZnMn$_2$O$_4$ < ZnAl$_2$O$_4$. This may be due to the variation of ionic radii of trivalent metal cation and the different cation distribution in the prepared spinels.

Table (3): FT-IR data, force constants, (K_T and K_O) and ($v_1 - v_2$) differences.

Sample	v_1 cm^{-1}	v_2 cm^{-1}	$K_T \times 10^5$ dyne/cm	$K_O \times 10^5$ dyne/cm	$v_1 - v_2$ cm^{-1}
$ZnAl_2O_4$	660	520	2.11	0.91	140
$ZnFe_2O_4$	544	390	1.35	0.49	154
$ZnCr_2O_4$	623	514	1.88	0.86	109
$ZnMn_2O_4$	624	515	1.89	0.89	109

3.3. SEM

SEM microstructure for the investigated samples is shown in Fig. 8. The SEM images of all samples showed sample surfaces composed of approximately irregular structures containing large pores as a result of the generation of large volume of gases during the combustion reaction which occurs in a very short time [36, 37]. As seen in Fig. 8a the SEM image of $ZnAl_2O_4$ shows aggregate plate's structure and spherical-shaped particles. The SEM image of $ZnFe_2O_4$ (Fig. 8b) shows the morphology of porous, sponge-like and agglomerated structure. the SEM image of $ZnCr_2O_4$ sample (Fig. 8c) shows particle with large aggregate plate's structure and cubic-shaped particles. The SEM image of $ZnMn_2O_4$ (Fig. 8d) sample shows particle with sponge-like and large aggregate plate's structure.
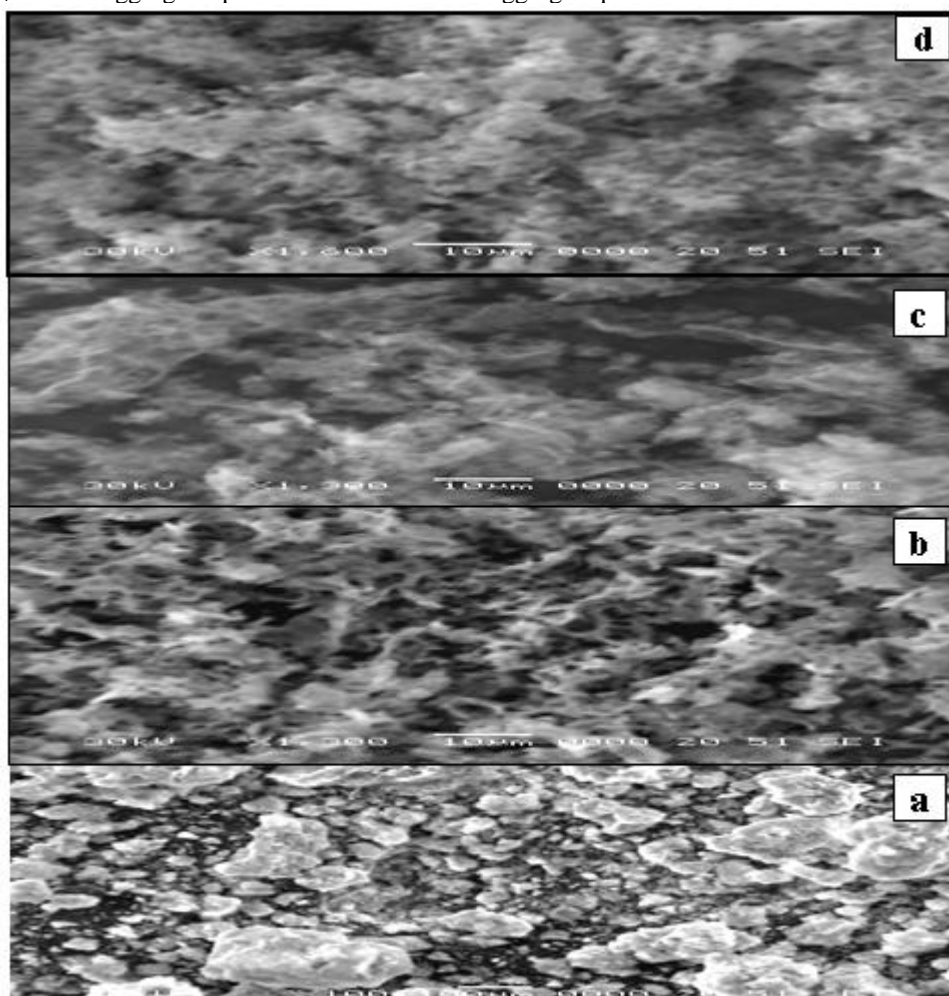

Fig. 8: SEM micrographs of (a) $ZnAL_2O_4$, (b) $ZnFe_2O_4$, (C) $ZnCr_2O_4$, (b) $ZnMn_2O_4$ prepared by combustion method.

3.4. TEM

TEM images of the investigated ZnM_2O_4, M= (Al, Fe, Cr, Mn) system are shown in Fig. 9. They show particle with different morphologies. The TEM – image of $ZnAl_2O_4$ sample (Fig. 9a) shows aggregation of spherical shapes and plate structures with particle size 20 nm. The TEM-image of the $ZnFe_2O_4$ sample (Fig. 9b), shows aggregation of nanorods of length 126 nm and width 8 nm and nanoplate particles with particle size 30 nm. Whereas, the morphology of the $ZnCr_2O_4$

sample, (Fig. 9c) shows aggregated particles of hexagonal and spherical structures with particle size 20 nm. Finally, the TEM-image of the $ZnMn_2O_4$ sample, (Fig. 9d) shows aggregated particles of rods structures with particle size

length 167 nm and width 15 nm. The particle sizes obtained are close to that estimated by XRD. The obviously determined lattice fringes show that the nanorod is basically single crystalline with no defect.
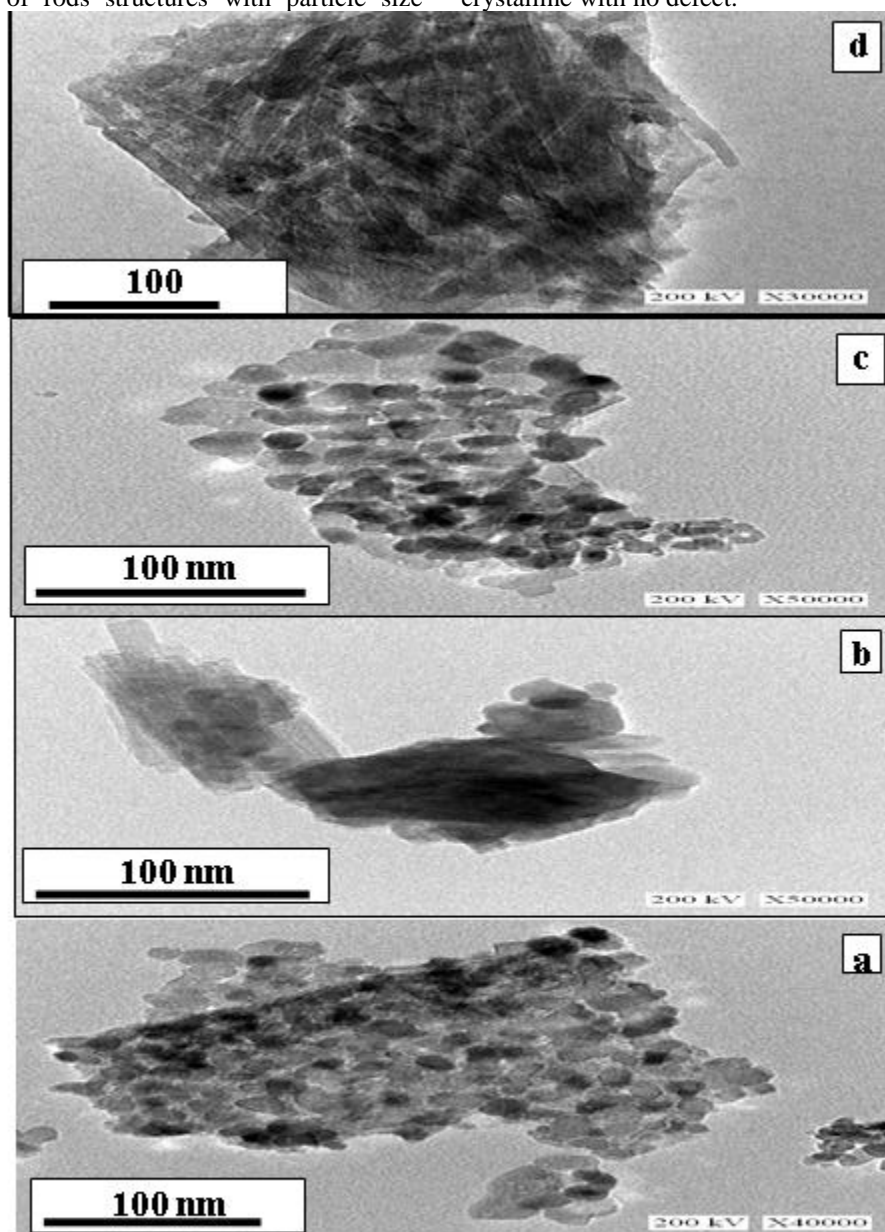

Fig. 9: TEM micrographs of (a) $ZnAl_2O_4$, (b) $ZnFe_2O_4$ (c) $ZnCr_2O_4$ (d) $ZnMn_2O_4$ prepared by combustion method.

4. Conclusion

Nano-crystalline ZnM_2O_4, M= (Al, Fe, Cr, Mn) particles have been prepared by combustion, hydrothermal and sol-gel methods. XRD patterns showed the best method for the preparation of the pure spinel structure is the combustion method. FT-IR carried out two absorption bands about 400 cm^{-1} and 600 cm^{-1} for octahedral and tetrahedral sites,

respectively, in all prepared samples by combustion method confirming the spinel structure. SEM and TEM reveal the formation of different morphological structure with different particle sizes (20-30 nm) depending on the composition of the sample.

References

[1] G. Blasse, Philips Res Report 28 (1968) 444-445.

[2] M. A. Mousa, M. A. Ahmed, Thermochim Acta 23 (1988) 3083-3087.

[3] M. A. Ahmed, J. Mater. Sci. Lett. 19 (2000) 791-794.

[4] K. Raj, R. Moskowitz, J. Magn. Magn. Mater. 85 (1990) 233-235.

[5] A. Moser, K. Takano, D.T. Margulies, M. Albrecht, Y. Sonobe, Y. Ikeda, S. Sun, J. Phys. D. Appl. Phys. 35 (2002) R157-R167.

[6] J. M. Bai, J. P. Wang, Appl. Phys. Lett. 87 (2004) 152502(1)-152502(3).

[7] R.C. Che, L. M. Peng, X. F. Duan, Q. Che , X. L. Liang, Adv. Mater. 16 (2004) 401-405.

[8] L. Gama, M. A. Ribeiro, B. S. Barros, R. H. Kiminami, I. T. Weber, A. C. Costa, J. Alloys and Compds. 483 (2009) 453-455.

[9] S. Kurajica, E. Tkalcec, J. Schmauch, J. Euro. Ceram. Soc. 27 (2007) 951-958.

[10] L. Giorgi, A. D. Bartolomeo, A. Brignocchi, J. Sol-Gel Sci. Technol. 26 (2003) 201-206.

[11] G. Sukul, D.V. Srinivasan, P.V. Balaramakrishna, J. Nano. Adv. Mat. 50 (2009) 328-336.

[12] M. Kutty, S. Dasgupta, S. Bandyopadhyay, Mate. Sci. 29 (2011) 121-126.

[13] F. LePeltier, P. Chaumette, J. Saussey, M. M. Bettahar, J. C. Lavalley, Mol. Catal. A. Chemical 122 (1997) 131-139.

[14] M. A. Valenzuela, P. Bosch, G. Aguilar-Rios, B. Zapata, C. Maldonado, I. Schifter, J. Mol. Catal. 84 (1993)177-186.

[15] E. M. Sanchez, M. G. Hipolito, M. Garcia, J. Guzman, F. R. Brito, J. S. Salazar, R. M. Martinez, O. A. Fregoso , M. I. Cortes , J. J. Delgado, C. Falcony, Phys. Stat. sol. 202 (2005) 102-107.

[16] W. S. Hong, L. C. Jonghe, J. Am. Ceram. Soc. 78 (1995) 3217-3224.

[17] G. Aguilar-Rios, M. Valenzuela, P. Salas, H. Armendariz, P. Bosch, G. Del Toro, R. Silva,V. Bertin, S. Castillo, A. Ramirez-Solis, I. Schifter, Appl. Catal. A. General 127 (1995) 65-75.

[18] M. A. Valenzuela, J. P. Jacobs, P. Bosch, S. Reijne, B. Zapata, H. H. Brongersma, Appl. Catal. A. General 148 (1997) 315-324.

[19] C. O. Arean, B. S. Sintes, G. T. Palomino, C. M. Carbonell, E. E. Platero, J. B. Soto, Microporous Mater. 8 (1997) 187-192.

[20] S. Guillemet-Fritsch, C. Chanel, J. Sarrias, S. Bayonne, A. Rousset , X. Alcobe, M. L. Martinez, Solid State Ionics 128 (2000) 233-242.

[21] G. Fierro, M. L. Jacono, R. Dragone, G. Ferraris, G. B. Andreozzi, G. Graziani, Appl. Catal. B. Environ. 57 (2005) 153-165.

[22] G. Ferraris, G. Fierro, M. L. Jacono, Appl. Catal. B. Environ. 36 (2002) 251-260.

[23] L. Q. Yan, W. Z. Jiang, X. D. Peng, L. H. He, F.W.Wang, Powder Diffr. 22 (2007) 340-343.

[24] X. Niu, W. Du, Sens. Actuators B 99 (2004) 405-409.

[25] Y. Yokomizo, S. Uno, M. Harata, H. Hiraki, K. Yuki, Sens. Actuators 4 (1983) 599-606.

[26] M. Bayhan, T. Hashemi, A.W. Brinkman, J. Mater. Sci. 32 (1997) 6619-6623.

[27] S. Pokhrel, B. Jeyaraj, K. S. Nagaraja, Mater. Lett. 57 (2003) 3543-3548.

[28] K. A. Alim, V. A. Fonoberov, M. Shamsa, A. A. Balandin, J. Appl. Phys. 97 (2005) 124313(1)-124313(5).

[29] H. P. Klug, L. E. Alexander, X-ray diffraction procedures for polycrystalline and amorphous materials. Wiley, New York (1970).

[30] M. C. Chhantbar, U. N. Trivedi, P. V. Tanna, H. J. Shah, R. P. Vara, H. H. Joshi, K. B. Modi, J. Phys. 78A (2004) 321-326.

[31] R. Lubbers, H. F. Grunsteudel, A. I. Chumakov, G. Wortmann, Science 287 (2000) 1250-1253.

[32] K. A. Mohammed, A. D. Al Rawas, A. M. Gismelseed, A. Sellai, H. M. Widatallah, A. Yousif, M. E. Elzain, M. Shongwe, Physica B 407 (2012) 795-804.

[33] K. A. Khalaf, A. D. Al-Rawas, H. M.Widatallah, A. Sellai, A. M. Gismelseed , M. Hashim, S. K. Jameel, M. S. Al-Ruqeishi, K. Al-Riyami, J. Alloy Comp. 657 (2016) 733-747.

[34] S. J. Yoon, S. H. Lee, K. H. Kim, K. S. Ahn, Mater. Chem. Phys. 73 (2002) 330-334.

[35] R. D. Waldron, Phys. Rev. 99 (1955) 1725-1727.

[36] L. A. Chick, L. R. Pederson, G. D. Maupin, J. L. Bates, Mater. Lett. 10 (1990) 6-12.

[37] T. Mimani, J. Alloys Compd. 315 (2001) 123-128.